

pubs.acs.org/NanoLett Letter

Unraveling the Structural Statistics and Its Relationship with Mechanical Properties in Metallic Glasses

Yu-Chia Yang, Zhenhai Xia, and Sundeep Mukherjee*



Cite This: https://doi.org/10.1021/acs.nanolett.1c02869



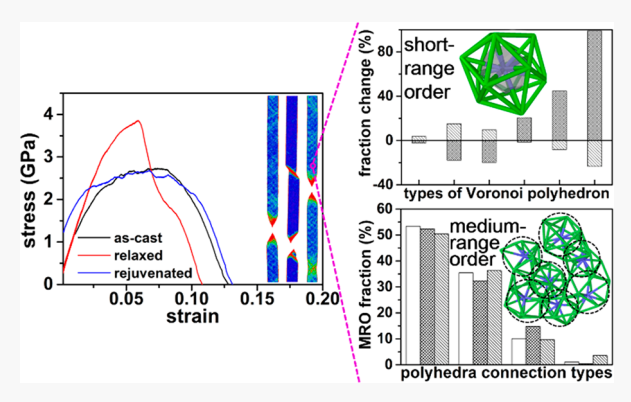
ACCESS

III Metrics & More

Article Recommendations

SI Supporting Information

ABSTRACT: Metallic glasses exhibit excellent properties such as ultrahigh strength and excellent wear and corrosion resistance, but there is limited understanding on the relationship between their atomic structure and mechanical properties as a function of their structural state. In this paper, we bridge the processing-structure-property gap by utilizing molecular dynamics simulation for a model binary metallic glass, namely $Ni_{80}P_{20}$. The structural statistics including the fraction of Voronoi index, the distribution of Voronoi volume, and medium-range ordering are calculated to explain the observed changes in mechanical behavior and strain localization upon relaxation and rejuvenation. Our findings demonstrate that the evolution of mechanical properties can be linked to the atomic structure change in terms of short- and mediumrange ordering. With the help of structural statistics, the mechanical properties are determined based on simple Voronoi analysis.



KEYWORDS: metallic glass, molecular dynamics, mechanical behavior, structural statistics, short-range order, medium-range order

1. INTRODUCTION

Metallic glasses (MGs) have attracted widespread scientific and technological interest because of their unique thermoplastic processing ability and excellent properties such as ultrahigh strength, wear and corrosion resistance, surface functionalization, and soft magnetism.¹⁻⁵ However, widespread use of metallic glasses, particularly in bulk form, is restricted because of their limited ductility. Thus, improving the mechanical properties of MGs in terms of ductility and toughness will likely result in a wide range of application areas well beyond the current niche. To address this challenge, it is necessary to understand the correlations between their atomic structure and mechanical properties with the goal of possibly tuning this relationship by appropriate processing. However, it is difficult to analyze the short-range order (SRO) and medium-range order (MRO) by experiments. With the help of molecular dynamics simulation, these local orderings may be statistically evaluated and distinguished by the types of polyhedra. Sheng et al. have made valuable contributions toward determining the stacking schemes in various amorphous alloys.^{6,7} Voronoi tessellation was carried out to investigate the SRO and quantify the frequency of dominant coordination polyhedra. Common neighbor analysis was utilized to explain the MRO and determine how the neighboring polyhedra are connected. In terms of statistical analysis, the local ordering network composed of different types of coordination polyhedra may be successfully delineated. Recently, the evolution of SRO and MRO has

been reported for Zr-based MGs as a function of heat treatment and mechanical preprocesses. 8-10 It was shown by Hwang et al. 10 that the individual type of polyhedron may be categorized into three major classes based on the fundamental geometry of each polyhedron, namely "icosahedral-like", "crystal-like", and "mixed" clusters. With such classification, the fraction change for the individual type of polyhedron is highly consistent in each class. However, there are knowledge gaps in the correlation between the evolution of atomic structure and mechanical properties in metallic glasses, particularly as a function of their structural state obtained by various processing routes. Fundamental insights into how relaxation and rejuvenation affect the SRO and MRO in amorphous alloys is clearly lacking.

Here, we bridge the processing-structure-property gap by analyzing SRO and MRO for as-cast, relaxed, and rejuvenated Ni₈₀P₂₀ metallic glass as a model amorphous alloy system. The Ni–P system was chosen because of its simple chemistry and application in a wide range of areas including automotive industries, surface protection from corrosion and wear, and micro/nanoelectromechanical systems (MEMS/NEMS).¹¹

Received: July 24, 2021
Revised: October 18, 2021



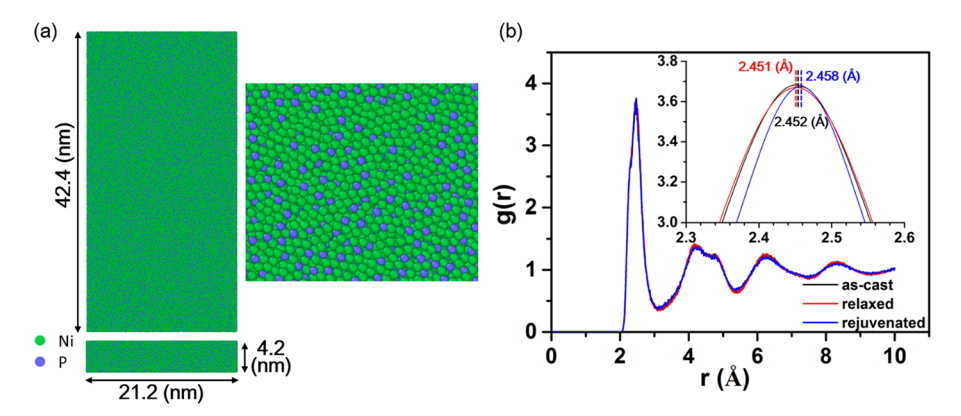


Figure 1. (a) Molecular model and magnified inset for $Ni_{80}P_{20}$ MG in the dimensions of $21.2 \times 42.4 \times 4.2$ (nm). The intended dimensions and aspect ratio are chosen to allow shear banding during mechanical deformation. (b) RDF curves for the as-cast, relaxed and rejuvenated MGs exhibiting typical pair distribution for amorphous alloys and indicating the distinct pair distance in SRO.

Adopting a refined and rigorous classification of structural statistics proposed by Sheng et al., we identified the coordination polyhedra for all the atoms in the model and classified them into two groups: (i) loose packing and (ii) dense packing. Our results show that the fraction of dense packing clusters increases while loose packing clusters decreases after structural relaxation, and this trend is completely reversed after rejuvenation. The observed embrittlement and localization of strain after relaxation is attributed to the loss of free volume enclosed by the loose packing atoms. In addition to SRO, MRO analysis was carried out to investigate the connections between the polyhedra and demonstrate their effect on mechanical properties. The loss in ductility for the relaxed model was explained by the decrease in edge-sharing and increase in face-sharing connections, whereas the increased toughness for the rejuvenated model was attributed to more edge-sharing and less face-sharing connections. Our findings reveal the relationship between the locally complex ordering in amorphous alloys and their corresponding mechanical properties. Structural statistics in SRO and MRO are treated as indicators to evaluate the mechanical performance.

2. METHODOLOGY

The simulations were performed by large-scale atomic/ molecular massively parallel simulator (LAMMPS) and an accurate Ni-P embedded atom model (EAM) potential was adapted from Sheng et al. The appropriate size of the model was selected to enable the nucleation and propagation of shear bands in the as-cast, relaxed, and rejuvenated Ni₈₀P₂₀ metallic glass. 12-14 The effect of aspect ratio was also studied 15 and the trend in mechanical properties was investigated as a function of their structural state obtained by the three processing routes. An initial model with fcc structure was melted at 2000 K and maintained for 2 ns. Afterward, an amorphous structure containing 345 600 atoms with dimensions $21.2 \times 42.4 \times 4.2$ nm was obtained from quenching a melted model at a rate of 1.0×10^{14} K/s. This high quench rate assured that the material was in a completely amorphous state. The glass transition temperature for Ni₈₀P₂₀ was determined to be 567 K from the change in slope of the potential energy versus temperature curve. The as-cast model was annealed at 560 (K) for 10 (ns) to obtain the relaxed model. The rejuvenated model was obtained by imposing a sinusoidal deformation with an amplitude of 10% strain and a period of 100 ps for 20 cycles.

The isothermal—isobaric (NPT) ensemble 16 based on the Nose—Hoover thermostat $^{17-19}$ and barostat were carried out for the heat treatment and mechanical processes. Periodic boundary conditions were imposed along x-, y-, and z-directions. Tensile and compressive tests were utilized to investigate the localized deformation and measurement of toughness. A nonperiodic boundary condition was enforced along the x-direction and the sample was deformed along the y-direction at a strain rate of $10^9~(s^{-1})$ until failure or the desired degree of deformation. For postprocessing analysis, OVITO was chosen as a visualization tool and some modifications, such as coordination analysis and Voronoi analysis, were added to identify the coordination polyhedra, clusters, Voronoi indices, and Voronoi volumes.

3. RESULTS AND DISCUSSION

3.1. Characteristics of MG Structures. The molecular model for Ni₈₀P₂₀ MG is shown in Figure 1a. The radial distribution function (RDF) for the as-cast, relaxed, and rejuvenated models (Figure 1b) are in good agreement with the expected amorphous structure. The first peak corresponds to SRO, indicating that the paired atoms are confined in certain type of polyhedra. Gaussian fitting was used for the first peak to differentiate the evolution of SRO upon structural relaxation and rejuvenation. As shown in the inset of Figure 1b, the peak is shifted to the left after relaxation of the MG and the distance of paired atoms in the first shell is reduced due to the atomic rearrangement. By contrast, the peak is shifted to the right and first shell distance is increased for the rejuvenated metallic glass. Thus, the change in the proportion of constituent polyhedra may be responsible for the SRO in MGs and may explain how the mechanical properties depend on the atomic structure. In addition, MRO, which is composed of the paired atoms in the second shell, may also play an important role. The connections among the polyhedra account for the second peak, resulting in a splitting of the RDF.²⁰ Generally, there are four ways to connect the neighboring polyhedra and form several clusters.^{20,21} Here, we evaluated the proportion change in each type of connection and demonstrated that MRO contributed to the change in mechanical properties after structural relaxation as well as rejuvenation.

3.1.1. Short-Range Order (SRO). The SRO was statistically analyzed by utilizing Voronoi tessellation for the as-cast, relaxed, and rejuvenated MGs and the Voronoi polyhedron is

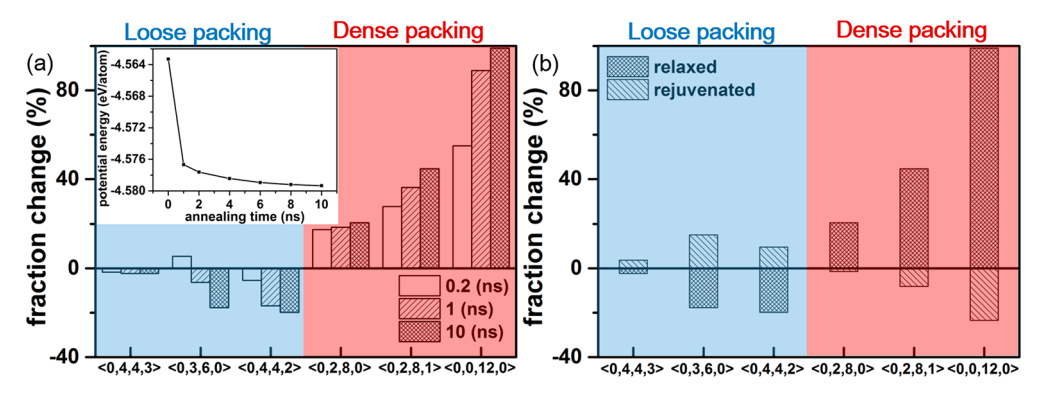


Figure 2. (a) Fraction change in each type of prevalent polyhedron as a function of annealing time. The inset is the potential energy of the MG as a function of annealing time, indicating a sharp decrease at the beginning of annealing followed by steady state. (b) Fraction change for the relaxed and rejuvenated models compared with the as-cast model.

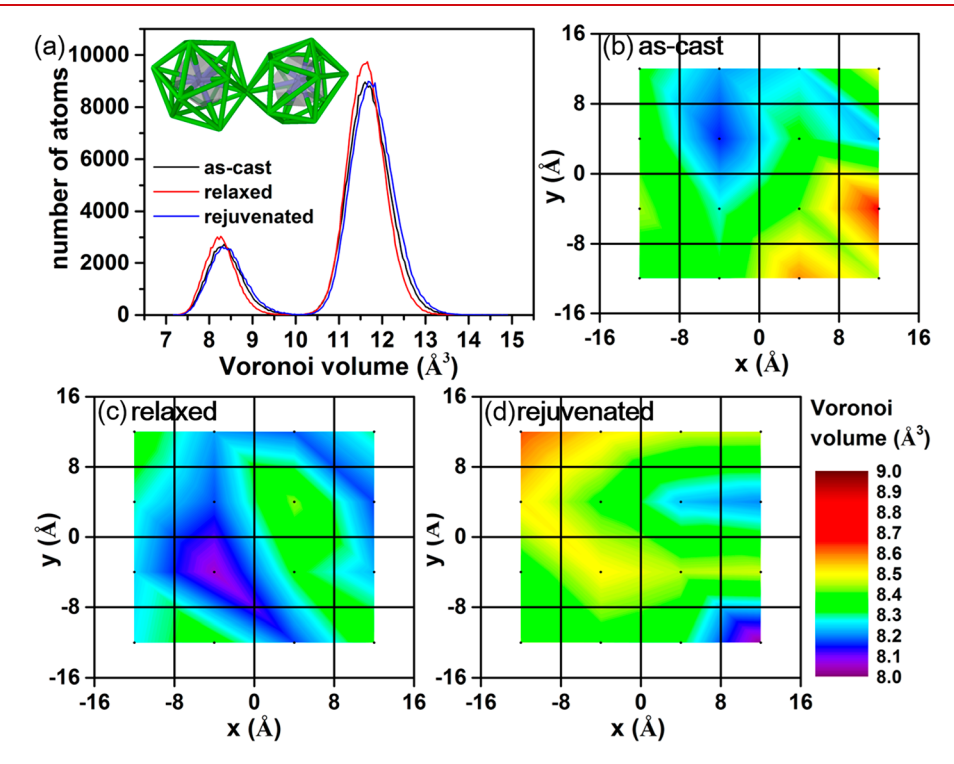


Figure 3. (a) Distribution of Voronoi volume, showing that the relaxed MG exhibits smaller and narrower volume distribution compared to the rejuvenated MG. Two Voronoi cells (gray) in P-centered icosahedra surrounded by Ni atoms are shown in the inset. Two-dimensional Voronoi volume distribution captured from the bulk model for (b) as-cast, (c) relaxed, and (d) rejuvenated MG. The relaxed MG shows relatively nonuniform distribution of free volume resulting in more localized deformation.

presented in the form of $\langle n_{3i}n_{4i}n_{5i}n_{6}\rangle$, where n_{i} refers to the number of surfaces with i edges. The criterion of classification is based on a previous report, separating all of the common polyhedra into two classes, namely loose packing and dense packing. Loose packing refers to the polyhedra with voids, whereas those with no voids are classified as dense packing. For each class, the three most prevalent and representative polyhedra were analyzed, and the fraction changes in the polyhedra are shown in Figure 2a. Three phases of the relaxed model with different annealing times of 0.2, 1, and 10 ns were calculated. The fraction change in individual polyhedra became larger with the increase in annealing time, except for (0,3,6,0). The reason may be that (0,3,6,x) is a group of polyhedra intermediate between loose packing and dense packing, which may be classified as "mixed"-type based on the geometry of this polyhedron. 10 The atomic rearrangement and structural

relaxation progressed at a rapid rate in the beginning of relaxation as shown in the inset of Figure 2a, indicating a sharp drop in potential energy within 1 ns followed by relatively steady decrease up to 10 ns.

As shown in Figure 2a, the fraction of polyhedra in loose packing decreased with an increase in annealing time whereas more ordered Kasper polyhedra are formed due to atomic rearrangement and are classified as dense packing clusters. Decreasing loose packing and increasing dense packing indicate annihilation of voids or free volume upon structural relaxation. Free volume in a metallic glass provides pathways for atomic diffusion and promotes plasticity. ^{22–24} Glasses with few dense packing atoms show lower energy barrier for atomic diffusion compared to the glassy state with many dense packing atoms. ⁷ Thus, the relaxed model with more dense packing atoms is likely to exhibit limited plasticity. In addition

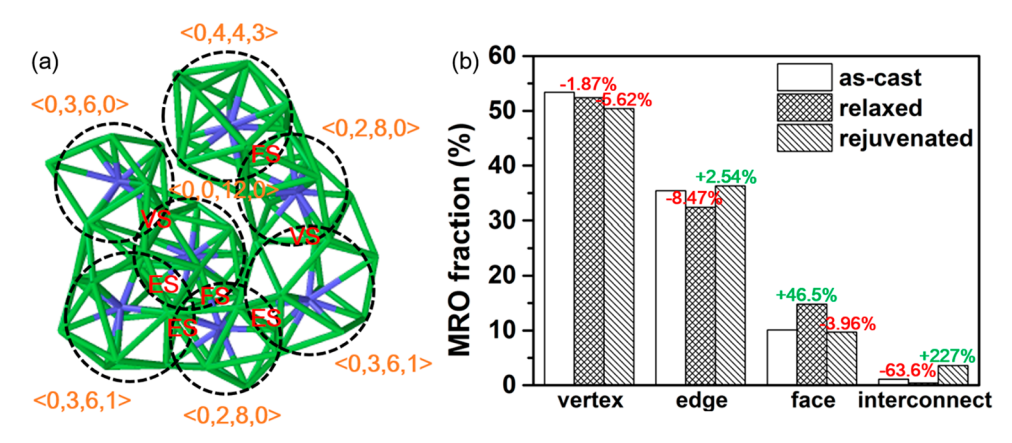


Figure 4. (a) A cluster composed of seven polyhedra, showing different types of connections that are indicated by the overlapping circles. (b) The MRO fraction for different types of connection, suggesting that the fraction of face-sharing connection with high stiffness increased while the edge-and interconnect-sharing decreased for the relaxed MG. The exact opposite trend was found for the rejuvenated MG.

to the change in loose packing and dense packing atoms that leads to embrittlement, we also observed that the amount of $\langle 0,2,8,0 \rangle$, $\langle 0,2,8,1 \rangle$, and $\langle 0,0,12,0 \rangle$ showed larger increments after relaxation. The fully icosahedral (0,0,12,0) cluster has been shown to increase Young's modulus but decrease plasticity. 25,26 The (0,2,8,0) polyhedron, also known as bicapped square antiprism (BSAP), and distorted BSAP (0,2,8,1) were found to be the dominant polyhedron for Ni₈₀P₂₀ MG, which is in line with previous reports.^{6,7} An increase in the number of dominant polyhedra not only promotes the formation of ordered structure but also reduces the disordered regions at which shear transformation is more likely to occur. Therefore, changes in mechanical properties may not only be correlated with changes in loose packing and dense packing groups but may also be attributed to some specific polyhedra. Figure 2b shows the fraction change in the different polyhedra for the relaxed and rejuvenated models. After rejuvenation, the MG exhibits exactly the opposite trend in loose packing and dense packing classes with an increase in free volume. Thus, mechanical rejuvenation may be expected to promote plasticity in MGs.

Voronoi volume was calculated for an icosahedron with a P atom at the center bonded to neighboring Ni atoms. The Voronoi polyhedron was determined by the intersection of perpendicular planes drawn at the midpoint of neighboring atoms. The distribution of Voronoi volume for the as-cast, relaxed, and rejuvenated model are shown in Figure 3a, with two peaks corresponding to P and Ni. Compared with as-cast Ni₈₀P₂₀ metallic glass, the distribution for the relaxed MG shifts to lower Voronoi volume, indicating shrinkage due to atomic rearrangement; however, a shift toward larger volume for the rejuvenated MG indicates locally dilated regions. These results are consistent with the RDF shown in Figure 1b. The volume distribution for the relaxed MG shows narrower but higher peaks compared to the as-cast model, indicating that the free volume is more concentrated and localized. The twodimensional (2D) distribution of Voronoi volume in 16 local regions is presented in Figure 3b-d for the as-cast, relaxed, and rejuvenated model, respectively. The dimensions of each local cube are $8 \times 8 \times 8$ Å, containing about 50 atoms with average cluster size that includes approximately four to five polyhedra. From Figure 3b-d, the average volume for the as-cast, relaxed and rejuvenated MG was calculated to be 8.367 ± 0.136 , 8.258 \pm 0.098, and 8.393 \pm 0.146 Å³, respectively. This represents

 \sim 1.3% decrease in free volume with relaxation and \sim 0.3% increase in free volume with rejuvenation. These results are in good agreement with that shown in Figure 3a, indicating smaller and narrower volume distribution in the relaxed MG but larger and wider distribution for the rejuvenated MG. Thus, the distribution of free volume in the relaxed MG is relatively nonuniform and shear flow is more likely to be concentrated in local regions, causing catastrophic failure. In contrast, more homogeneous flow is expected in the rejuvenated MG since shear deformation is sustained by more regions with larger Voronoi volume.

3.1.2. Medium-Range Order (MRO). To statistically investigate the paired atoms in the second shell, the connection between two P-centered polyhedra was evaluated to determine the MRO in Ni₈₀P₂₀ metallic glass. Typically, there are four types of connections between neighboring polyhedra, namely vertex-sharing (VS), edge-sharing (ES), face-sharing (FS), and interconnected-sharing (IS). 20,21 The number of sharing atoms for these connection types are 1, 2, 3 and 4, respectively. Here, we studied all clusters composed of the prevalent coordination polyhedra and one of the clusters is presented in Figure 4a, showing a size of seven polyhedra and connections indicated by two overlapping circles. By inspecting the clusters one by one, we were able to obtain the fraction of polyhedral connections. Figure 4b shows the fraction for each type of polyhedral connection in the as-cast, relaxed, and rejuvenated MG. After structural relaxation, the fraction of face-sharing increased while edge- and interconnect-sharing decreased. The fraction change after rejuvenation was in the opposite direction. According to the results by Ding et al., 20 facesharing is the most favored connection when an MG transitions from liquid state to glassy state. The clusters with more face-sharing would show higher stiffness while those with more edge- and interconnected-sharing would exhibit better flexibility.

3.2. Mechanical Properties of the MGs and Their Correlation with the MG Structure. Von Mises shear strain was used to investigate the local deformation and shear localization in the as-cast, relaxed, and rejuvenated Ni₈₀P₂₀ MG under compressive stress imposed along the *y*-direction (as shown in Figure S1a). The shear strain distribution at different applied strains is shown in Figure S1. At a strain of 5%, there were more local regions where flow was initiated in the as-cast and rejuvenated MG than the relaxed one. In contrast, for the

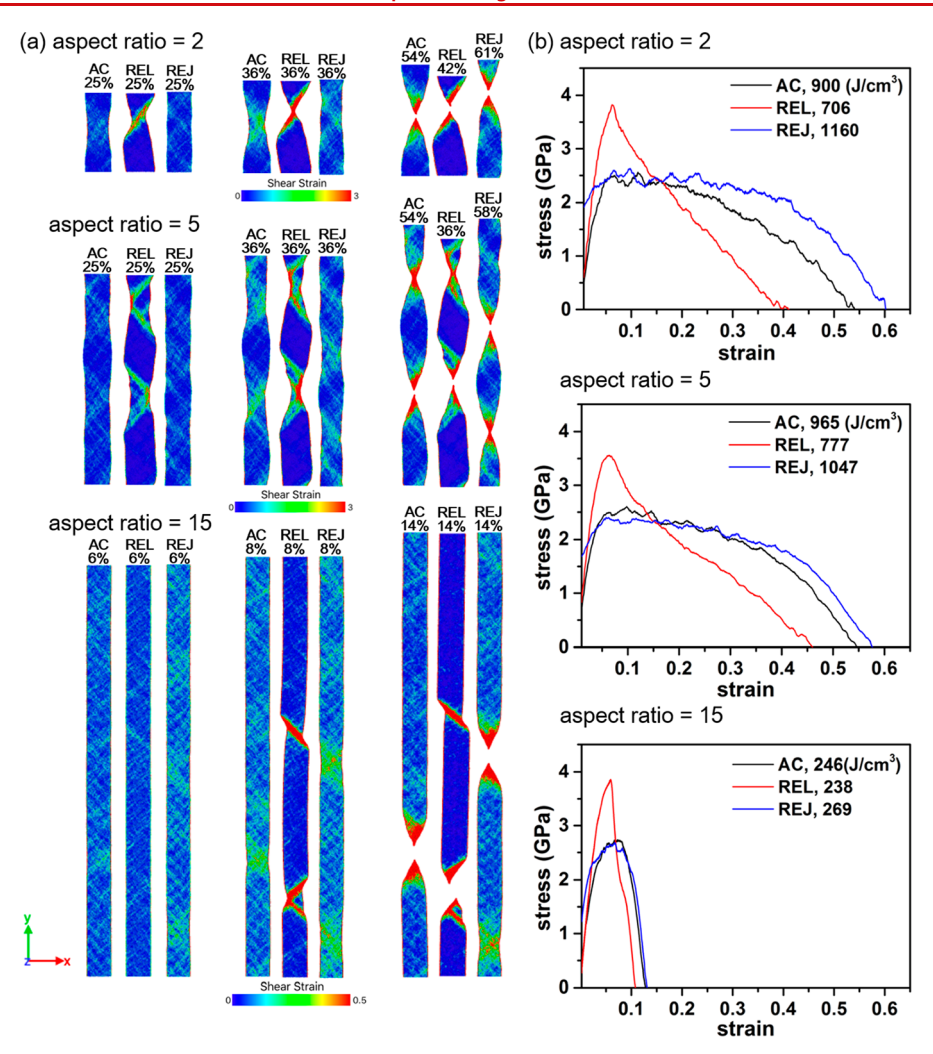


Figure 5. (a) Von Mises shear strain for the AC, REL, and rejuvenated REJ models with aspect ratio equal to 2, 5, and 15 at different strains as marked on the figures. (b) Stress—strain curves for the three models with different aspect ratios, showing similar trend in deformation behavior, strain at failure, and fracture energy (indicated next to the structural state in the legend). The model pillars with aspect ratio of 15 showed relatively more brittle characteristics compared to the pillars with aspect ratio of 2 and 5.

relaxed MG the shear strain was induced only in certain local regions because of nonuniform distribution of free volume and less clusters with flexible polyhedral connections. At a strain of 10%, there was relatively homogeneous deformation in the ascast and rejuvenated MG. In contrast, the regions with maximum shear deformation developed into obvious shear localization for the relaxed MG. At strains of 20% and 50%, the deformation in rejuvenated MG was largely homogeneous, and only a limited degree of strain localization was identified in the as-cast MG. For the relaxed MG, well-developed shear localization was observed, causing unevenness on the surface of the *x*-plane. Videos showing the deformation of the MGs are included in the Supporting Information (the scale of strain is fixed during compression).

Tensile tests were conducted on the model pillars for three different aspect ratios of 2, 5, and 15 with dimensions of $13.6 \times (13.6 * aspect ratio) \times 1.7$ nm, to calculate the fracture energy (toughness) from the corresponding stress—strain curves. Figure 5a shows the evolution in shear strain for different aspect ratios, and Figure 5b shows the corresponding stress—strain curves for the as-cast (AC), relaxed (REL), and rejuvenated (REJ) MGs (the aspect ratio for each set is marked on the figure). The model pillars with aspect ratio of

15 showed relatively more brittle characteristics compared to the pillars with aspect ratio of 2 and 5. This may be attributed to rapid propagation of shear bands in high aspect ratio pillars in contrast to relatively slower moving shear bands in low aspect ratio pillars. 15 In addition, the pillars with aspect ratio of 2 showed a single region of shear localization in contrast to multiple failure points for the pillars with aspect ratio of 5 and 15. Taking the intermediate aspect ratio of 5, necking occurred in the relaxed sample at the strain of 25% due to strong shear localization, whereas the as-cast and rejuvenated MGs showed relatively homogeneous deformation behavior at the same strain. At 36% strain, some degree of shear localization was observed in both as-cast and rejuvenated MGs because shear flow was eventually confined in some "weak" regions with relatively large free volume. For the rejuvenated MG, strain was more distributed in numerous local regions. Finally, the rejuvenated MG with an aspect ratio of 5 fractured at the strain of 58%, showing higher ductility compared to the corresponding as-cast and relaxed models. As seen in Figure 5b, the relaxed MG exhibited higher elastic modulus and yielding stress than the as-cast MG because of larger fraction of (0,0,12,0) polyhedra and face-sharing connections with greater stiffness due to the atomic rearrangement. Table S1 in

Supporting Information lists the overall changes in atomic structure and Table S2 lists the corresponding mechanical properties obtained from tensile tests of MG pillars with different aspect ratios. The fracture energy calculated for the MG pillar with aspect ratio of 5 based on area under the stress-strain curves were 965, 777, and 1047 (J/cm³) for the as-cast, relaxed, and rejuvenated models, respectively. The trend in fracture energy remained the same for the Ni₈₀P₂₀ metallic glass pillars irrespective of the three aspect ratios studied, that is, rejuvenated > as-cast > relaxed. The value of fracture energy is listed next to the structural state of the metallic glass in Figure 5b legend as well as summarized in Table S2. This clearly demonstrates that toughening in metallic glasses may be achieved by increasing the fraction of loose packing in SRO, decreasing the fraction of dense packing, creating more edge- and interconnected-sharing connections within MRO, and reducing the fraction of face-sharing connections.

4. CONCLUSIONS

The structural characteristics of as-cast state, relaxed state, and rejuvenated Ni₈₀P₂₀ MG were analyzed using molecular dynamics simulation and correlated with their mechanical behavior. The structures of the three states were characterized by (1) the size of the first shell in RDF, (2) the fraction change and categorization of prevalent polyhedra, (3) Voronoi volume change, and (4) the fraction and types of polyhedra connection. Upon relaxation, the voids or free volume were annihilated due to the decrease of polyhedra in loose packing group and increase in dense packing group. In addition, increase in BSAP and fully icosahedral polyhedron was found to promote inhomogeneous flow. The rejuvenated MGs had relatively large and uniform free volume distribution giving rise to homogeneous flow, whereas shear flow was concentrated in small regions causing catastrophic failure in relaxed MGs. Structural relaxation increased the fraction of face-sharing connections with greater stiffness, which increased the yield strength but reduced the ductility. Our results show that Voronoi indices are useful indicators in evaluating the mechanical behavior as a function of structural statistics. This work provides a theoretical basis for understanding the evolution in short- and medium-range order in metallic glasses to help guide the processing routes for tailoring their mechanical properties and vastly expanding their potential application areas beyond the niche.

ASSOCIATED CONTENT

Supporting Information

The Supporting Information is available free of charge at https://pubs.acs.org/doi/10.1021/acs.nanolett.1c02869.

Von Mises shear strain distribution during compression, table with summary of short-range order (SRO), and medium-range order (MRO) fraction, and table with summary of mechanical properties (PDF)

Video of molecular dynamics simulation of the compression test of metallic glass model pillars (MP4)

AUTHOR INFORMATION

Corresponding Author

Sundeep Mukherjee – Department of Materials Science and Engineering, University of North Texas, Denton, Texas 76203, United States; orcid.org/0000-0002-1954-0045; Email: sundeep.mukherjee@unt.edu

Authors

Yu-Chia Yang — Department of Materials Science and Engineering, University of North Texas, Denton, Texas 76203, United States

Zhenhai Xia — Department of Materials Science and Engineering, University of North Texas, Denton, Texas 76203, United States; ⊙ orcid.org/0000-0002-0881-2906

Complete contact information is available at: https://pubs.acs.org/10.1021/acs.nanolett.1c02869

Notes

The authors declare no competing financial interest.

ACKNOWLEDGMENTS

This work was supported by funding from the National Science Foundation (NSF) under Grants 1561886, 1919220, 1762545, and 1662288.

REFERENCES

- (1) Inoue, A. Stabilization of metallic supercooled liquid and bulk amorphous alloys. *Acta Mater.* **2000**, *48*, 279–306.
- (2) Ma, M. Z.; et al. Wear resistance of Zr-based bulk metallic glass applied in bearing rollers. *Mater. Sci. Eng., A* **2004**, *386*, 326–330.
- (3) Telford, M. The case for bulk metallic glass. *Mater. Today* **2004**, 7. 36–43.
- (4) Arora, H. S.; et al. Wettability of nanotextured metallic glass surfaces. *Scr. Mater.* **2013**, *69*, 732–735.
- (5) Shao, Z.; Gopinadhan, M.; Kumar, G.; Mukherjee, S.; Liu, Y.; O'Hern, C. S.; Schroers, J.; Osuji, C. O. Size-dependent viscosity in the super-cooled liquid state of a bulk metallic glass. *Appl. Phys. Lett.* **2013**, *102*, 21901.
- (6) Sheng, H. W.; et al. Atomic packing and short-to-medium-range order in metallic glasses. *Nature* **2006**, 439, 419–425.
- (7) Sheng, H. W.; Ma, E.; Kramer, M. J. Relating Dynamic Properties to Atomic Structure in Metallic Glasses. *JOM* **2012**, *64*, 856–881.
- (8) Feng, S. D.; et al. A molecular dynamics analysis of internal friction effects on the plasticity of $Zr_{65}Cu_{35}$ metallic glass. *Mater. Eng.* **2015**, *80*, 36–40.
- (9) Feng, S. D.; et al. Rejuvenation by weakening the medium range order in $Zr_{46}Cu_{46}Al_8$ metallic glass with pressure preloading: A molecular dynamics simulation study. *Mater. Des.* **2018**, *158*, 248–255
- (10) Hwang, J.; et al. Nanoscale Structure and Structural Relaxation in Zr₅₀Cu₄₅Al₅ Bulk Metallic Glass. *Phys. Rev. Lett.* **2012**, *108*, 195505.
- (11) Sadeghilaridjani, M.; et al. Multiscale Manufacturing of Amorphous Alloys by a Facile Electrodeposition Approach and Their Property Dependence on the Local Atomic Order. *ACS Appl. Mater. Interfaces* **2021**, *13*, 9260–9271.
- (12) Song, H. Y.; Li, S.; Deng, Q. Coupling effects of thickness and aspect ratio on deformation behavior of Cu₅₀Zr₅₀ metallic glass. *Comput. Mater. Sci.* **2017**, *139*, 106–114.
- (13) Luan, Y. W.; et al. Plastic deformation mechanisms and size effect of Cu₅₀Zr₅₀/Cu amorphous/crystalline nanolaminate: A molecular dynamics study. *Comput. Mater. Sci.* **2017**, *129*, 137–146.
- (14) Li, Q.-K.; Li, M. Assessing the critical sizes for shear band formation in metallic glasses from molecular dynamics simulation. *Appl. Phys. Lett.* **2007**, *91*, 231905.
- (15) Sopu, D.; et al. Brittle-to-Ductile Transition in Metallic Glass Nanowires. *Nano Lett.* **2016**, *16*, 4467–4471.
- (16) Martyna, G. J.; Tobias, D. J.; Klein, M. L. Constant pressure molecular dynamics algorithms. J. Chem. Phys. 1994, 101, 4177.

- (17) Shinoda, W.; Shiga, M.; Mikami, M. Rapid estimation of elastic constants by molecular dynamics simulation under constant stress. *Phys. Rev. B: Condens. Matter Mater. Phys.* **2004**, *69*, 134103.
- (18) Hoover, W. G.; Holian, B. L. kinetic moments method for the canonical ensemble distribution. *Phys. Lett. A* **1996**, 211, 253–257.
- (19) Hoover, W. G. Canonical dynamics: Equilibrium phase-space distributions. *Phys. Rev. A: At., Mol., Opt. Phys.* **1985**, 31, 1695.
- (20) Ding, J.; Ma, E.; Asta, M.; Ritchie, R. O. Second-Nearest-Neighbor Correlations from Connection of Atomic Packing Motifs in Metallic Glasses and Liquids. *Sci. Rep.* **2015**, *5*, 17429.
- (21) Luo, W. K.; Sheng, H. W.; Ma, E. Pair correlation functions and structural building schemes in amorphous alloys. *Appl. Phys. Lett.* **2006**, *89*, 131927.
- (22) Spaepen, F. A microscopic mechanism for steady state inhomogeneous flow in metallic glasses. *Acta Metall.* **1977**, 25, 407–415.
- (23) Argon, A. S. Plastic deformation in metallic glasses. *Acta Metall.* **1979**, 27, 47–58.
- (24) Bokeloh, J.; Divinski, S. V.; Reglitz, G.; Wilde, G. Tracer Measurements of Atomic Diffusion inside Shear Bands of a Bulk Metallic Glass. *Phys. Rev. Lett.* **2011**, *107*, 235503.
- (25) Cheng, Y. Q.; Sheng, H. W.; Ma, E. Relationship between structure, dynamics, and mechanical properties in metallic glass-forming alloys. *Phys. Rev. B: Condens. Matter Mater. Phys.* **2008**, 78, 014207.
- (26) Park, K. W.; et al. Atomic packing density and its influence on the properties of Cu–Zr amorphous alloys. *Scr. Mater.* **2007**, *57*, 805–808.